IDENTIFICATION OF SUB-SURFACE DEFECTS IN PARTS PRODUCED BY ADDITIVE MANUFACTURING, USING LASER GENERATED ULTRASOUND

Sarah K. Everton[1,2], Phill Dickens[1], Chris Tuck[1], Ben Dutton[2]

[1] Additive Manufacturing and 3D Printing Research Group, University of Nottingham, University Park, Nottingham, NG7 2RD, UK.
[2] The Manufacturing Technology Centre, Ansty Business Park, Pilot Way, Coventry, Warwickshire, CV7 9JU, UK.

Keywords: Laser ultrasound, laser ultrasonic testing, defect characterisation, non-destructive testing, additive manufacturing

Abstract

Additive manufacturing (AM) offers a number of benefits over manufacture by conventional means, giving an increased design freedom and the opportunity to integrate multiple components, saving weight. The rigorous standard for material integrity set by the Aerospace and Medical sectors necessitates the development of systems to ensure the quality of AM components is sufficient.

Laser ultrasonic testing (LU) is a non-contact inspection technique which might be well suited for in-situ monitoring of AM processes, as measurements can be taken on curved surfaces and at elevated temperatures. In this paper, the results of a recent study looking to generate and identify sub-surface defects in samples produced by laser powder bed fusion are shared. Samples with defects replicating those commonly resulting from processing by AM have been seeded and analysed post-process, in order to establish the limits of detection for LU and to assess the suitability of this technique for in-situ inspection of AM.

Introduction

Additive manufacturing (AM) as a technology has matured rapidly in recent years and is now being commercially exploited across many manufacturing sectors, as is reported each year in the Wohler's report [1]. Several aerospace engine manufacturers have looked to AM to reduce component weight, leadtimes and cost [2], however component integrity is still a concern. In the UK, a steering group representing AM users in both the private and public sectors identified a lack of robust processes as a key barrier to the wider adoption of AM, in particular the lack of in-situ monitoring [3, 4]. Similarly, the US National Institute of Standards and Technology highlighted "in-situ data acquisition, in order to enable closed-loop control and detection of material discontinuities", as a priority area for research and development [5].

AM is defined in the American Society for Testing and Materials (ASTM) standard F2792 as "the process of joining materials to make objects from 3-D model data, usually layer upon layer, as opposed to subtractive manufacturing technologies" [6]. This standard also outlines the seven different process families grouped under the AM heading. A comprehensive introduction to AM is given by Gibson et al. [7]. As referenced above, it is the development of metal powder bed fusion (PBF) processes which are currently being championed by the aerospace sector. PBF can be categorised further, based on utilisation of a laser or an electron beam energy source. The two processes are inherently similar and as such, resulting materials yield similar deficiencies.

The laser PBF process has over fifty input parameters, some of which are interdependent [8]. In order to produce components with sufficient material integrity for the aerospace sector, an understanding of the effect of changing these parameters is required and, as such, many studies have been undertaken [9, 10]. A wide range of "defects" are known to occur during AM processing, the most common of which are material discontinuities such as pores, inclusions and cracks [11].

Pores are significant, as they reduce the effective load carrying capacity of a material and also act as stress concentrators, providing effective crack initiation sites [12]. Pores can be further categorised by size, shape and content such as "spherical, gas filled" [13], "elongated, powder filled" [14, 15] or "keyhole" pores [16], see Figure 1.

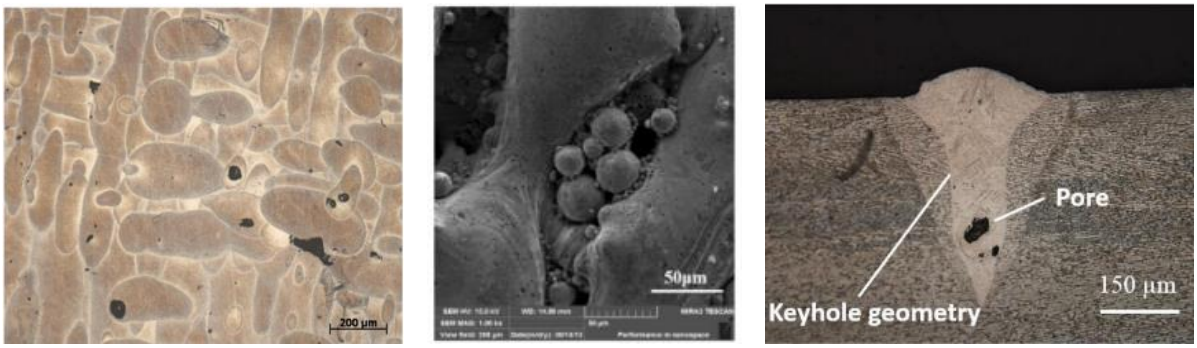

Figure 1 - Showing spherical pores (left) [14], unmelted powder (centre) [17] and keyhole pore (right) [15].

Ideally, these defects would be eradicated as process understanding matures and a tighter control of input parameters is achieved. However, for applications where material integrity must be ensured, in-situ monitoring will allow for identification of any defects during manufacture. Many non-destructive, monitoring methods for laser-PBF and electron beam-PBF have been explored to date to aid process understanding [18], but could also be implemented for in-situ inspection. Thermographic [19-22] and visual monitoring methods [23-28] are common, but are limited to observing only the surface of the AM build. Ultrasonic devices would enable sub-surface inspection, but are limited by their inability to operate on rough, AM surfaces, irregularly shaped objects and at high temperatures. Laser generated ultrasound (LU) is well suited to in-situ inspection of AM processes. Laser techniques are non-contacting, thus do not exhibit any coupling problems; they can be used for rapid scanning and are amenable to use in hostile environments.

Although LU has been shown to be capable of detecting the types of defects generated during additive manufacture [29, 30], there have been a limited number of experiments applying laser ultrasonic inspection directly to additively manufactured materials [31-33]. In order to test any inspection system for identification of AM defects, representative samples must be manufactured and, therefore, the generation mechanisms for each defect type must be understood.

In a previous study, LU was successfully trialled on both AM as-built and AM post processed surfaces and with artificial "defects", manufactured by wire electron discharge machining (EDM). In this study, an analysis of LU has been carried out on samples manufactured by laser PBF with seeded, powder filled voids. The LU results have been compared with x-ray computed tomography (XCT) to assess building samples in this way and to trial the LU system with AM representative surfaces; the initial results are presented here.

Laser ultrasonic testing

Background

A typical LU system comprises a pulsed laser to generate ultrasonic waves, a continuous-wave detection laser, an interferometer, an oscilloscope and a PC (Figure 2 - left). Ultrasonic wave generation results from absorption of the incident laser light pulse and energy conversion through a thermoelastic process, resulting in ultrasonic waves. At high energy densities, a plasma forms at the surface of the material which produces an impulsive recoil force after the plasma expands, generating ultrasonic waves; this is termed the ablation regime [34]. In order to detect a material discontinuity, the laser pulse is directed at the sample surface and ultrasonic waves propagate along and into the sample.

The dominant wave mode generated is a surface wave, also termed a Rayleigh wave (R), however compression/longitudinal (L) and bulk/shear (S) waves are also generated [35]. The waves, travelling with different velocities travel directly between the generation and detection lasers, but also reflect off the bottom, ends and sides of a sample (Figure 2 - right). Time of flight (TOF) calculations can be carried out to estimate the arrival times of the various waves, once the material and geometry of the sample are known; these times can be used to ensure the correct LU set-up is selected so that waves do not interact unnecessarily.

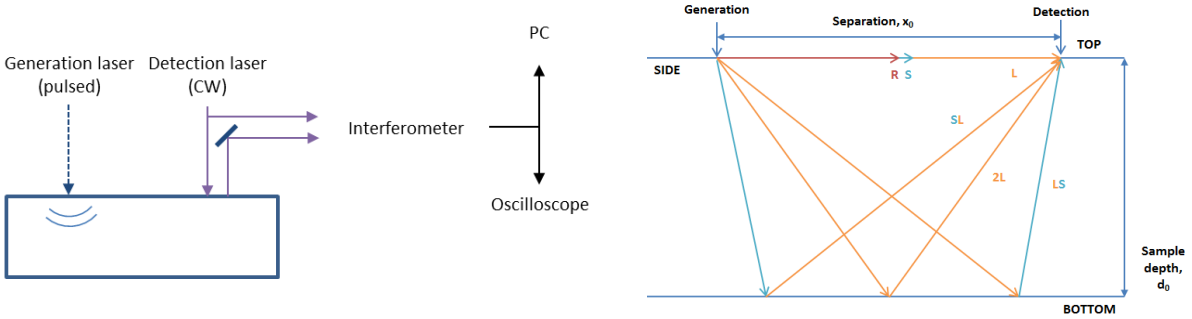

Figure 2 - Schematic of LU set-up (left) and of wave paths from top to bottom of sample (right).

Where a sub-surface defect is present between the generation and detection lasers, the Rayleigh wave diffracts and scatters and upon its return to a receiver is comprised of shear waves and mode converted longitudinal waves. The detection laser receives the returned signal which is then processed to provide details about the feature of interest.

There are a number of ways in which ultrasonic data can be displayed. A snapshot, termed an A-scan (Figure 3 - left) is produced at each scanning location, which displays the received ultrasonic energy at the detection point, as a function of time. For LU systems with a motorised linear stage, a snapshot is taken at defined distance intervals along the top of the sample and the series of A-scans are compiled and stacked to create a profile view of the sample, termed a B-scan – (Figure 3 - right).

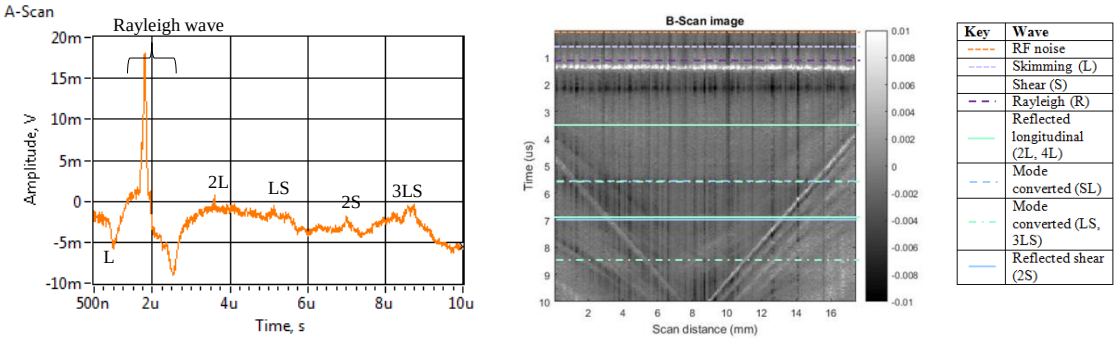

Figure 3 - A typical A-scan, extracted from LaserScan (left) and predicted wave arrival times overlaid on an B-scan with key (right).

As the generation and detection laser are moved across the surface at a fixed distance, any interaction with a defect results in a parabolic indication on the B-scan, in the region of the Rayleigh wave; it is this period which will be analysed in this study.

Equipment

The LU system used at the Manufacturing Technology Centre (MTC) is mostly contained within an interlocking enclosure and is operated remotely using the computer or integrated hardware such as the generation laser wand. The generation laser is a class IV, Q-switched Nd:YAG laser with a wavelength of 1064 nm, capable of delivering 200 mJ energy with each 20 ns pulse at 20 Hz frequency. The pumping and cooling units are positioned outside the enclosure and the laser head mounted on a motorised stage within. The detection laser is a 1550 nm +/- 10 nm wavelength fibre laser which operates in continuous wavelength mode with a maximum output power of 10W. The accompanying 'Analogue Processing Module' contains a temporal differentiator for high-pass filtering and a linear, low-noise amplifier. A 'Continuously Variable Fibre Power Splitter' and 'Guide Beam' module allows for a 0-100 % division of power into the probe beam (mounted in the measurement head) and the reference beam which is outputted to the interferometer. The guide beam injects a red laser beam into the probe fibre so that the probe beam can be visualised safely for alignment purposes. The generation laser and detection laser fibre fed optics are mounted within the measurement head and the beam separation can be adjusted remotely from 0-100 mm. The measurement head can be operated at a stand off from 80-230 mm from the workpiece and the spot sizes can be adjusted using interchangeable lenses with varying focal lengths. The measurement head can be adapted so that in-line or side-by-side scans can be taken of the sample which is placed below.

Test Samples

Samples were designed with spherical voids below the surface at various depths. The effect of the PBF as-built surface finish on the LU signal detection was also investigated. Blocks of Titanium alloy Ti-6Al-4V were produced by laser PBF on a Realizer SLM50 machine, using 40 µm layers, 100 W power, 20 µm point distance, 40 µs exposure and 90 µm hatch spacing; a double scan strategy was also employed (Figure 4 - centre).

10 *x* 30 *x* 10 mm blocks with multiple voids were manufactured for this study with a "defect free" zone ahead of four evenly spaced 200 µm voids, at 250 or 500 µm below the top surface (Figure 4 - left). A solid AM block and a block made from billet were also made to use for reference. The samples were placed under the LU system and the measurement head mounted such that in-line measurements could be taken at 0.1 mm intervals, along the centre of the sample in the x-direction (Figure 4 - right). Results taken from the blocks will be discussed below.

Figure 4 - Schematic of block with seeded defects (left), SLM50 processing of samples (centre) and photographs showing start and end laser positions for LU (right).

Results

Laser Ultrasonic Testing

The B-scans generated using Matlab from the LU data are shown below, along with an example A-scan for each block. As the received AC signal from the detector is dependent on light being reflected from the sample surface, at positions of low light, the AC value will be low; dividing by the average DC value at each point normalises this effect.

As expected, the billet reference block did not indicate the presence of any defects and returned a much smaller amplitude signal (Figure 5); this is due to the smoother, less reflective EDM surface. The solid AM reference block also gives no indication of any defects (Figure 6). The AM block with seeded defects shows indications of defects in the region between 2.5 and 15 mm (Figure 7), after the initial Rayleigh wave peak. Further processing will reveal additional information regarding the shape, depth or size of any present defects.

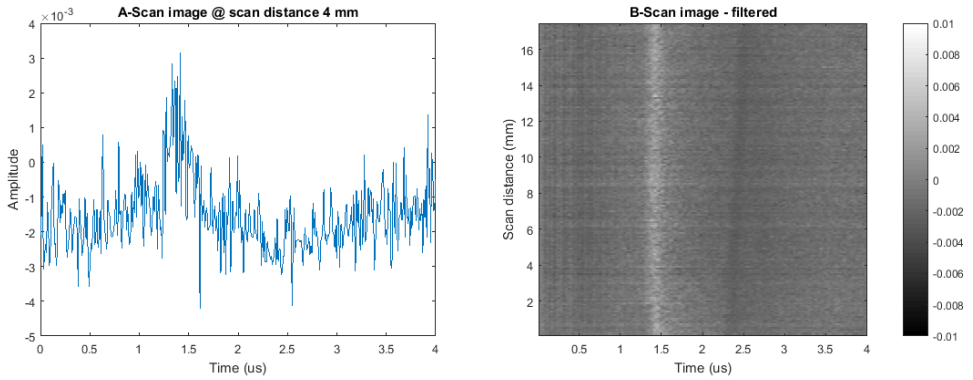

Figure 5 - A-scan at 4 mm (left) and B-scan (right) - Billet reference block.

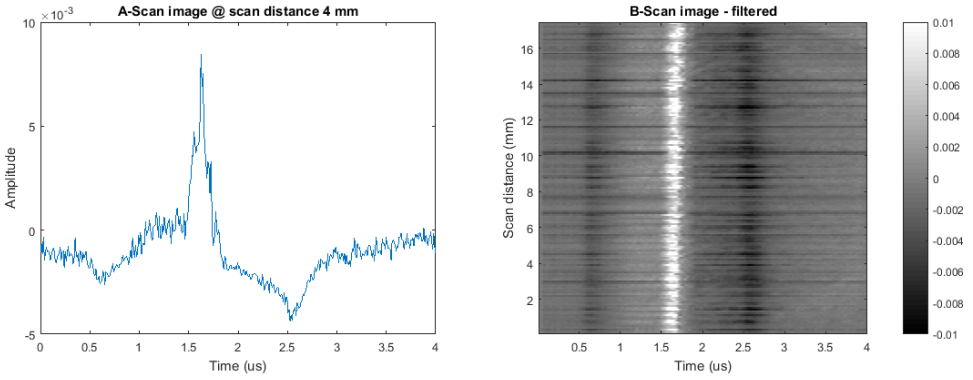

Figure 6 – A-scan at 4 mm (left) and B-scan (right) - AM reference block.

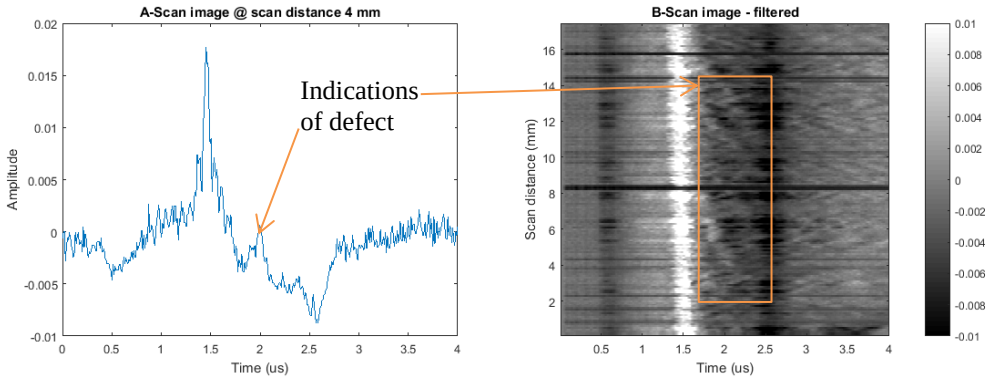

Figure 7 - A-scan at 4 mm (left) and B-scan (right) – AM seeded defect block.

Previously, when LU trials were carried out with EDM through holes, rather than enclosed "voids", the presence of the four defects was distinct, unlike in this instance where it is unclear.

X-ray Computed Tomography

In order to interrogate the AM seeded defect block further, a Nikon XT H 225 XCT system was used to image the samples with 27 µm voxel size. As anticipated from the LU scans, XCT images of the billet and AM reference blocks did not reveal any indicated defects (Figure 8). The circled areas in the images in Figure 9 indicate where a defect was intended to be seeded in the AM seeded defect block. Analysis of these images gives no suggestion that a defect was in fact formed in the seeded area, although other unintended porosity is apparent which might have caused the indications seen using LU.

Figure 8 - XCT image of AM solid block sample (x-y plane at 250 µm from top surface).

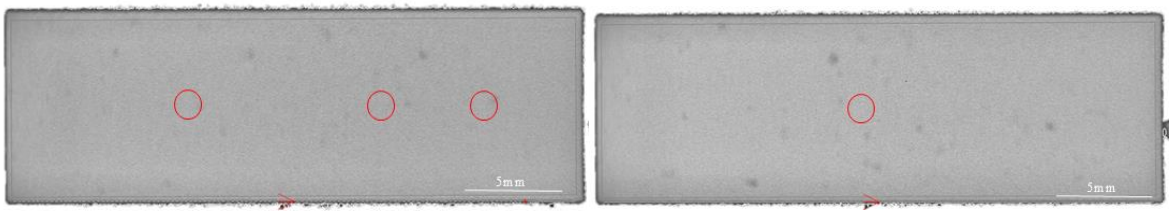

Figure 9 - XCT image of AM block showing intended locations of seeded defects - x-y plane at 250 µm from top surface (left) and x-y plane at 500 µm from top surface (right).

Automated defect recognition (ADR) software built into the VGStudio MAX 2.2 package was used to further assess the AM block with seeded defects, in order to explain the indications seen during LU. Seven large voids with diameters between 610 µm and 860 µm were returned, see Figure 10. Two of these seven defects (circled), are located sufficiently close to the top surface and along the central channel which was traversed by the lasers, to explain the indications given by LU. Work continues to correlate the data gathered by LU and XCT.

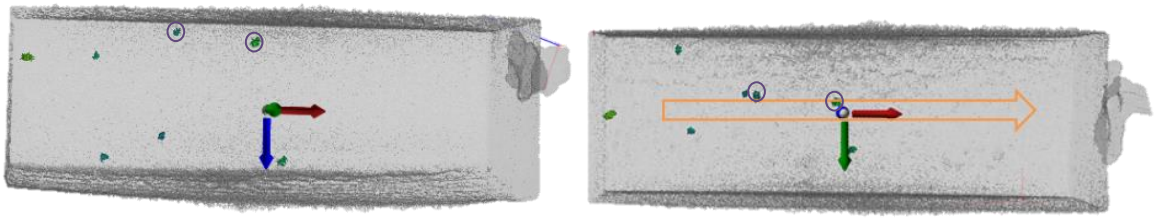

Figure 10 - ADR images showing locations of defects within the blocks from a side view (left) and from the top view (right). The circled defects are within the approximate LU scanning channel, shown with an arrow.

Conclusions

Seeding defects is not straight forward; simply leaving a void in the AM sample model does not necessarily result in a defect, due to the layer-wise nature of AM processing. It is possible that during manufacture, the seeded voids were "healed" when processing subsequent layers or that the voids contain partially sintered powder allowing the waves to penetrate, unaffected.

For LU, although filtering and signal averaging were employed, the signal received was still noisy. Further interrogation of the data is required, including more advanced filtering, in order to gain meaningful results. Destructive analysis would support the XCT results generated using ADR. Nevertheless, the LU system has been successful in detecting sub-surface imperfections in an as-built, laser PBF sample.

Future Work

In addition to the work outlined above, a series of samples will instead be generated with 'naturally occurring defects'. Laser scan speed and hatch spacing will be manipulated to create a 'defect zone' within a block of highly dense material, close to the top surface. The LU system will be used to assess these samples.

Acknowledgements

The primary author is working within the Manufacturing Technology Engineering Doctorate Centre, supported by the Manufacturing Technology Centre, University of Nottingham and the Engineering and Physical Sciences Research Council under Award No. 1361477. Work has been carried out in conjunction with FP7-2012-NMO-ICT-FoF project 313781, AMAZE.

References

1. Wohlers, T.T., *Wohlers Report 2015*. Vol. 22. 2015: Wohlers Associates.
2. Nathan, S., *Aerospace takes to additive manufacturing*, in *The Engineer*. 2015, Centaur Communications Ltd. Available from: https://www.theengineer.co.uk/aerospace-takes-to-additive-manufacturing/
3. Additive Manufacturing Steering Group UK, *Steering Group*. 2015; Available from: http://www.amnationalstrategy.uk/steering-group/.
4. Additive Manufacturing Special Interest Group, *Shaping our national competency in additive manufacturing*, T.S. Board, Editor. 2012, UK Government. Available from: https://connect.innovateuk.org/documents/2998699/3675986/UK+Review+of+Additive+Manufacturing+-+AM+SIG+Report+-+September+2012.pdf/a1e2e6cc-37b9-403c-bc2f-bf68d8a8e9bf.
5. Energetics Incorporated, *Measurement science roadmap for metal-based additive manufacturing*. 2013, National Institute of Standards and Technology: Maryland, US. .
6. ASTM Standard, *Standard terminology for additive manufacturing technologies*, in *ASTM Standard F2792-12a*. 2012, ASTM International: West Conshohocken, PA.
7. Gibson, I., Rosen, D.W. and Stucker, B., *Additive Manufacturing Technologies: Rapid Prototyping to Direct Digital Manufacturing*. 2009: Springer.
8. Van Elsen, M., *Complexity of selective laser melting: A new optimisation approach*, (P.D. theses, Katholieke Universiteit Leuven: Belgium, 2007). p. 31-42.
9. Gong, H., et al., *Influence of defects on mechanical properties of Ti–6Al–4 V components produced by selective laser melting and electron beam melting.* Materials & Design, 2015. **86**: p. 545-554.
10. Tammas-Williams, S., et al., *XCT analysis of the influence of melt strategies on defect population in Ti–6Al–4V components manufactured by selective electron beam melting.* Materials Characterization, 2015. **102**(4): p. 47-61.
11. Aboulkhair, N.T., et al., *Reducing porosity in AlSi10Mg parts processed by selective laser melting*. Additive Manufacturing, 2014. **1–4**: p. 77-86.

12. Brandl, E., et al., *Additive manufactured AlSi10Mg samples using Selective Laser Melting (SLM): Microstructure, high cycle fatigue, and fracture behavior.* Materials & Design, 2012. **34**: p. 159-169.
13. Monroy, K., Delgado, J. and Ciurana, J., *Study of the pore formation on CoCrMo alloys by selective laser melting manufacturing process.* Procedia Engineering, 2013. **63**: p. 361-369.
14. Kempen, K., et al., *Process optimization and microstructural analysis for selective laser melting of AlSi10Mg*, in *Solid Freeform Fabrication Symposium*. 2011: Austin, TX.
15. Gong, H., et al., *Melt pool characterization for selective laser melting of Ti-6Al-4V pre-alloyed powder*, in *Solid Freeform Fabrication Symposium*. 2014: Austin, TX.
16. King, W.E., et al., *Observation of keyhole-mode laser melting in laser powder-bed fusion additive manufacturing.* Journal of Materials Processing Technology, 2014. **214**(12): p. 2915-2925.
17. Zhou, X., et al., *3D-imaging of selective laser melting defects in a Co–Cr–Mo alloy by synchrotron radiation micro-CT.* Acta Materialia, 2015. **98**: p. 1-16.
18. Everton, S.K., et al., *Review of in-situ process monitoring and in-situ metrology for metal additive manufacturing.* Materials & Design, 2016. **95**: p. 431-445.
19. Schwerdtfeger, J., Singer, R.F., and Körner, C., *In situ flaw detection by IR-imaging during electron beam melting.* Rapid Prototyping Journal, 2012. **18**(4): p. 259-263.
20. Rodriguez , E., et al., *Integration of a thermal imaging feedback control system in electron beam melting*, in *Solid Freeform Fabrication Symposium*. 2012: Austin, TX.
21. Price, S., et al., *Experimental temperature analysis of powder-based electron beam additive manufacturing*, in *Solid Freeform Fabrication Symposium*. 2013: Austin, TX.
22. Krauss, H., Eschey, C., and Zaeh, M.F., *Thermography for monitoring the selective laser melting process*, in *Solid Freeform Fabrication Symposium*. 2012: Austin, TX.
23. Scharowsky, T., et al., *Observation and numerical simulation of melt pool dynamic and beam powder interaction during selective electron beam melting* in *Solid Freeform Fabrication Symposium*. 2012, UT, Austin: Austin, TX.
24. Berumen, S., et al., *Quality control of laser- and powder bed-based Additive Manufacturing (AM) technologies.* Physics Procedia, 2010. **5**(Part B): p. 617-622.
25. Craeghs, T., et al., *Detection of process failures in layerwise laser melting with optical process monitoring.* Physics Procedia, 2012. **39**(1): p. 753-759.
26. Craeghs, T., et al. *Online quality control of selective laser melting*. in *Solid Freeform Fabrication Symposium*. 2011. Austin, TX.
27. Lott, P., et al., *Design of an optical system for the in situ process monitoring of selective laser melting (SLM).* Physics Procedia, 2011. **12**(Part A): p. 683-690.
28. Kleszczynski, S., et al. *Error detection in laser beam melting systems by high resolution imaging*. in *Solid Freeform Fabrication Symposium*. 2012. Austin, TX.
29. Edwards, R.S., et al., *Scanning laser source and scanning laser detection techniques for different surface crack geometries*, in *Review of Progress in Quantitative Nondestructive Evaluation*. 2012, AIP Conference Proceedings: Burlington, VT. p. 251-258.
30. Klein, M., Sienicki, T., and Eichenbergeer, J., *Laser-ultrasonic detection of subsurface defects in processed metals.* Patent: US7278315. 2007: United States.
31. Everton, S., et al. *Evaluation of laser ultrasonic testing for inspection of metal additive manufacturing*. in *SPIE*. 2015. San Francisco, CA. US.
32. Santospirito, S.P., et al. *Defect detection in laser powder deposition components by laser thermography and laser ultrasonic inspections*. in *SPIE*. 2013. San Diego, CA.
33. Cerniglia, D., et al., *Inspection of additive-manufactured layered components.* Ultrasonics, 2015. **62**: p. 292-298.
34. Sarrafzadeh, A., Churchill, R., and Niimura, M., *Laser Generated Ultrasound*, in *Acousto-Ultrasonics*. 1988, Springer. p. 201-207.
35. Edwards, R.S., Dutton, B., and Clough, A.R., *Interaction of laser generated ultrasonic waves with wedge-shaped samples.* Applied Physics Letters, 2012. **100**(18): p. 184102.